Magneto-thermal properties and slow magnetic relaxation in Mn(II)Ln(III) complexes: Influence of magnetic coupling on the magneto-caloric effect

ARTICLE

Magneto-thermal properties and slow magnetic relaxation in Mn(II)Ln(III) complexes: Influence of magnetic coupling on the magneto-caloric effect

Itziar Oyarzabal,*[a,b] Andoni Zabala-Lekuona,[c] Antonio J. Mota,[d] María A. Palacios,[d] Antonio Rodríguez-Diéguez,[d] Giulia Lorusso,[e] Marco Evangelisti,*[f] Corina Rodríguez-Esteban,[a] Euan K. Brechin,[g] José M. Seco*[c] and Enrique Colacio*[d]

A family of Mn(II)Ln(III) dinuclear and tetranuclear complexes (Ln = Gd and Dy) has been prepared from the compartmental ligands N,N'-dimethyl-N,N'-bis(2-hydroxy-3-formyl-5-bromobenzyl)ethylenediamine (H₂L¹) and N,N',N''-trimethyl-N,N''-bis(2-hydroxy-3-methoxy-5-methylbenzyl)diethylenetriamine (H₂L²). The Mn(II)Gd(III) complexes exhibit antiferromagnetic interactions between Mn(II) and Gd(III) ions in most cases, which are supported by Density Functional Theory (DFT) calculations. Experimental magneto-structural correlations carried out for the reported complexes and other related complexes found in bibliography show that the highest ferromagnetic coupling constants are observed in di-μ-phenoxido bridged complexes, which is due to the planarity of the Mn-(μ-O)₂-Gd bridging fragment and to the high Mn-O-Gd angles. The effect of these angles has been studied by DFT calculations performed on a di-μ-phenoxido doubly bridged model. The magneto-thermal properties of the Mn(II)Gd(III) based complexes have also been measured, concluding that the magnitude of the Magneto-Caloric Effect (MCE) is due to the strength rather than to the nature of the magnetic coupling. Moreover, when two Mn(II)Gd(III) dinuclear units are connected by two carbonato-bridging ligands the MCE is enhanced, obtaining a maximum magnetic entropy change of 36.4 Jkg⁻¹K⁻¹ at ΔB = 7 T and T = 2.2 K. On the other hand, one of the dinuclear Mn(II)Dy(III) complexes displays Single-Molecule Magnet (SMM) behaviour with an energy barrier of 14.8 K under an applied external field of 1000 Oe.

Introduction

Molecular Magnetism based on coordination compounds directs currently its research attention to materials exhibiting amazing magnetic properties such as Single-Molecule Magnets (SMMs)[1] and low-temperature magnetic coolers,[2] among others. SMMs are nanomagnets that overlap the quantum/classical borderline as they display classical properties, such as slow relaxation of magnetization and magnetic hysteresis below the so-called blocking temperature (T_B), as well as quantum properties such as quantum tunnelling of the magnetization (QTM) and quantum phase interference.[1] This exceptional combination of physical properties makes

them good candidates for potential future applications, among other areas, in ultra-high density magnetic information storage,[3] molecular spintronics,[4] and as qubits for quantum computing at molecular level.[5]

The SMM behaviour comes from the existence of an energy barrier (U_{eff}) for the magnetization reversal, which essentially depends on the magnetic anisotropy of the system.[1] As lanthanide ions exhibit strong magnetic anisotropy, they have been widely employed in the preparation of SMMs, obtaining a large number of 3d/4f clusters and 4f metal complexes that exhibit this behaviour, most of them containing Dy ions.[6] In this regard, the highest T_B values (close to the boiling point of liquid nitrogen) and coercive fields have been observed in monometallic metallocene Dy derivatives and mixed-valence dilanthanide (Ln = Dy or Tb) complexes with metal-metal bonding.[7] It is interesting to note that 3d/4f systems usually possess lower energy barriers and blocking temperatures than the monometallic and low-nuclearity 4f metal complexes. The behaviour observed for 3d-4f systems is due to the effective shielding of the fully occupied 5s and 5p orbitals to the 4f orbitals of the Ln(III) ions, which leads to very weak 3d-4f magnetic exchange interactions and therefore, to multiple low-lying excited states.[8] In addition, the random transversal field created by the paramagnetic metal ions on the Ln(III) ions can also contribute to the worsening of the SMM behaviour, as it favours the QTM process.[9] In spite of the above considerations,

[a.] BCMaterials, Basque Center for Materials, Applications and Nanostructures, UPV/EHU Science Park, 48940 Leioa. Email: Itziar.oyarzabal@bcmaterials.net
[b.] IKERBASQUE, Basque Foundation for Science, 48009 Bilbao, Spain.
[c.] Departamento de Química Aplicada, Facultad de Química, Universidad del País Vasco/Euskal Herriko Unibertsitatea (UPV/EHU), 20018 Donostia, Spain. Email: josemanuel.seco@ehu.eus
[d.] Departamento de Química Inorgánica, Facultad de Ciencias, Universidad de Granada, 18071 Granada, Spain. Email: ecolacio@ugr.es
[e.] CNR - Istituto per la Microelettronica e Microsistemi, Unità di Bologna, 40129 Bologna, Italy.
[f.] Instituto de Nanociencia y Materiales de Aragón (INMA), CSIC-Universidad de Zaragoza, 50009 Zaragoza, Spain. Email: marevacre@unizar.es
[g.] EaStCHEM School of Chemistry, The University of Edinburgh, David Brewster Road, Edinburgh EH9 3FJ, UK.
Electronic Supplementary Information (ESI) available: crystallographic data, SHAPE measurements results, additional magnetic and magneto-caloric data. See DOI: 10.1039/x0xx00000x

Journal Name   **ARTICLE**

the Cr(III)Dy(III) based complex $[Cr(III)_2Dy(III)_2(OMe)_2(O_2CPh)_4(mdea)_2(NO_3)_2]$ (H_2mdea = N-methyldiethanolamine)[10] is an example of how the incorporation of isotropic paramagnetic ions can improve the SMM properties when compared to the diamagnetic Co(III) based analogue, which is due to the fact that the exchange interaction between the Dy(III) and Cr(III) ions is unusually strong, leading to a multilevel exchange type barrier[11] and to the suppression of the QTM. However, in the Co(III) based compound the barrier originates only from one excited state on the individual Dy(III) ions.

On the other hand, heteropolynuclear 3d-Gd(III) complexes have been the focus of several magneto-thermal studies as they can display potential applications as low temperature magnetic coolers.[2] This is so because the change of magnetic entropy observed in these and other coordination complexes upon application of a magnetic field, which is called magneto-caloric effect (MCE), can be exploited for molecular refrigeration[2] and, therefore, coordination complexes have emerged as good candidates to replace the rare and expensive He-3 as cryogenic coolers. In contrast to SMMs, the MCE is enhanced in molecules containing isotropic magnetic ions that exhibit weak magnetic interactions between the metal ions, as this generates multiple low-lying excited and field-accessible states that can contribute to the magnetic entropy of the system. Taking this into account, complexes containing the isotropic Gd(III) ion, which has the maximum entropy value calculated as $R\ln(2S_{Gd} + 1)/M_{Gd}$ = 110 $Jkg^{-1}K^{-1}$ and 3d transition metals complexes such as Mn(II), Fe(III), Cr(III) and Cu(II) would be good candidates for molecular refrigeration. Among them, Mn(II) should be, in principle, the best choice as it has the maximum entropy value of 271 $Jkg^{-1}K^{-1}$ and lower oxidation state than Fe(III) ion, which has also d^5 electronic configuration (a lower oxidation state generally implies that a less number of non-magnetic ligands are required to balance the charge). The primary target in this field is to obtain metal complexes with MCE as high as possible. In this regard, it is very helpful to investigate experimentally in a systematic way and with simple compounds the effects of the sign and magnitude of the magnetic coupling between the metal ions on the MCE.

In this article we present the synthesis, structural characterization and magnetic properties of a series of closely related Mn(II)Ln(III) dinuclear and tetranuclear complexes (Ln = Gd and Dy) with the compartmental ligands N,N'-dimethyl-N,N'-bis(2-hydroxy-3-formyl-5-bromobenzyl)ethylenediamine (H_2L^1) and N,N',N''-trimethyl-N,N''-bis(2-hydroxy-3-methoxy-5-methylbenzyl)diethylenetriamine (H_2L^2). It is worth mentioning that Mn-Ln complexes containing only Mn(II) ions are quite uncommon compared to Mn(III)–Ln(III) and Mn(III)/Mn(II)–Ln(III) counterparts.[12] The aim of this work is threefold: (i) To establish magneto-structural correlations for the simple Mn(II)Gd(III) dinuclear complexes; (ii) To analyze how magneto-thermal properties of this family of closely related Mn(II)Gd(III) based compounds are influenced by the magnitude and sign of the magnetic exchange coupling and (iii) To know if the large anisotropy of the Dy(III) ions, together with the coupling to

paramagnetic isotropic Mn(II) ions, could lead to the presence of SMM behaviour in the Dy(III) derivatives.

Experimental

Materials and methods

All reactions were performed under ambient laboratory atmosphere, with the reagents purchased from commercial sources and used without further purification. Ligands H_2L^1 and H_2L^2 were prepared according to previously described procedures.[13]

Synthetic procedures

$[Mn(\mu-L^1)(\mu-OAc)Ln(NO_3)_2]\cdot CH_3CN\cdot H_2O$, Ln = Gd (1), Dy (2). To a solution of 30.6 mg (0.125 mmol) of $Mn(OAc)_2\cdot 4H_2O$ in 5 mL of acetonitrile/methanol mixture (80:20) were added with continuous stirring 64.3 mg (0.125 mmol) of H_2L^1 and 0.125 mmol of the corresponding $Ln(NO_3)_3\cdot nH_2O$. The resulting yellow solution was filtered and allowed to stand at room temperature. After few days, well-formed prismatic yellow crystals of **1** and **2** were obtained with yields of 32 and 26 %, respectively. Anal. Calcd. for $C_{24}H_{28}N_5O_{13}Br_2MnGd$: C, 29.82; H, 2.92; N, 7.25. Found: C, 29.91; H, 2.93; N, 7.29. Anal. Calcd. for $C_{24}H_{28}N_5O_{13}Br_2MnDy$: C, 29.66; H, 2.90; N, 7.21. Found: C, 29.71; H, 2.91; N, 7.23.

$[Mn(CH_3OH)(\mu-L^2)Dy(NO_3)_3]$ (3). To a solution of H_2L^2 (55.7 mg, 0.125 mmol) in 5 mL of MeOH were subsequently added with continuous stirring 31.4 mg (0.125 mmol) of $Mn(NO_3)_2\cdot 4H_2O$ and 54.8 mg (0.125 mmol) of $Dy(NO_3)_3\cdot 5H_2O$. The resulting pistachio green solution was filtered and allowed to stand at room temperature. After several days, well-formed prismatic white crystals of $[Mn(CH_3OH)(\mu-L^2)Dy(NO_3)_3]$ (**3**) were obtained with a yield of 51 %. Anal. Calcd. for $C_{26}H_{41}N_6O_{14}MnDy$: C, 35.52; H, 4.70; N, 9.56. Found: C, 35.61; H, 4.68; N, 9.59.

$[Mn(\mu-L^2)(\mu-OAc)Ln(NO_3)_2]$, Ln = Gd (4), Dy (5). 30.6 mg (0.125 mmol) of $Mn(OAc)_2\cdot 4H_2O$ and 0.125 mmol of the corresponding $Ln(NO_3)_3\cdot nH_2O$ were successively added to a solution of H_2L^2 (55.7 mg, 0.125 mmol) in 5 mL of MeOH. The resulting solution was stirred during 30 minutes and then was filtered to eliminate any amount of insoluble material. The filtrate was allowed to stand at room temperature for several days, whereupon colourless X-ray quality crystals were formed. Yields: 15 and 17 % respectively for **4** and **5**. Anal. Calcd. for $C_{27}H_{40}N_5O_{12}MnGd$: C, 38.66; H, 4.81; N, 8.35. Found: C, 38.71; H, 4.78; N, 8.39. Anal. Calcd. for $C_{27}H_{40}N_5O_{12}MnDy$: C, 38.42; H, 4.78; N, 8.30. Found: C, 38.51; H, 4.79; N, 8.39.

$[Mn(\mu-L^2)(\mu-9-An)Ln(NO_3)_2]\cdot 2CH_3CN$, Ln = Gd (6), Dy (7). To a solution of H_2L^2 (55.7 mg, 0.125 mmol) in 5 mL of CH_3CN were subsequently added 31.4 mg (0.125 mmol) of $Mn(NO_3)_2\cdot 4H_2O$ and 0.125 mmol of the corresponding $Ln(NO_3)_3\cdot nH_2O$ with continuous stirring. To this solution was added dropwise another solution of CH_3CN containing 27.8 mg of 9-anthracenecarboxylic acid (0.125 mmol) and 12.6 mg of triethylamine (0.125 mmol), which was filtered off and left to stand at room temperature, obtaining X-ray quality crystals. Yields: 36 and 42 % respectively for **6** and **7**. Anal. Calcd. for

$C_{44}H_{52}N_7O_{12}MnGd$: C, 48.79; H, 4.84; N, 9.05. Found: C, 48.81; H, 4.88; N, 9.09. Anal. Calcd. for $C_{44}H_{52}N_7O_{12}MnDy$: C, 48.56; H, 4.82; N, 9.01. Found: C, 48.61; H, 4.79; N, 9.03.

{(μ_3-CO$_3$)$_2$[Mn(μ-L^2)Gd(NO$_3$)]$_2$}·(CH$_3$OH)$_2$·H$_2$O (8) and {(μ_3-CO$_3$)[Mn(μ-L^2)Gd(NO$_3$)]$_2$}·(CH$_3$OH)$_2$ (9). To a hot (50 °C) methanolic solution (10 mL) of H_2L^2 (28.0 mg, 0.0625 mmol), $Mn(NO_3)_2$·4H$_2$O (15.7 mg, 0.0625 mmol) and the corresponding $Ln(NO_3)_3$·nH_2O (0.0625 mmol), Et_3N (0.017 mL, 0.125 mmol) was added. Then, Na_2CO_3 (6.6mg, 0.0.0625 mmol) was added dropwise, which was dissolved in the minimum amount of distilled water prior to the addition. The solution was immediately filtered while hot affording colourless crystals of **8** and **9** in few minutes.

Powder X-ray diffraction and thermogravimetric measurements revealed a fast loss of crystallization solvents after filtering off the crystals (Fig. S1-S4), which based on the physical properties measurements (vide infra) did not significantly impact the structure of the tetranuclear compounds. Moreover, elemental analysis results agree well with the values expected for the unsolvated analogues and there is no appreciable weight loss until ~ 250 °C, which leads to $LnMnO_3$ (Expected weight percentage for $GdMnO_3$: 35.7 %. Observed: 35 %, Fig. S4). Yields for the unsolvated compounds: 18 and 49 % respectively for **8** and **9**. Anal. Calcd. for $C_{52}H_{74}N_8O_{20}Mn_2Gd_2$: C, 40.15; H, 4.79; N, 7.20. Found: C, 40.35; H, 4.78; N, 7.29. Anal. Calcd. for $C_{52}H_{74}N_8O_{20}Mn_2Dy_2$: C, 39.88; H, 4.76; N, 7.16. Found: C, 40.01; H, 4.83; N, 7.04.

Physical measurements

Elemental analyses were carried out on a Leco CHNS-932 microanalyzer. Thermogravimetric analysis (TGA) were performed on a TG-Q500 TA Instruments thermal analyser under a synthetic air atmosphere (79 % N$_2$ / 21 % O$_2$) at a heating rate of 10 °C min^{-1}. Variable-temperature magnetic susceptibility, magnetization and alternating-current (*ac*) susceptibility measurements were carried out with Quantum Design SQUID MPMS XL5, Quantum Design SQUID MPMS-7 T, CFMS-VSM-14 T (CryoFree Magnet System – Vibrating Sample Magnetometer) and PPMS (Physical Property Measurement System) – Quantum Design Model 6000 magnetometers. Diamagnetic corrections were estimated from the Pascal's constants. Heat capacity measurements were carried out for **8**, using a Quantum Design PPMS, equipped with a ^{3}He cryostat, on a thin pressed pellet (ca. 1 mg) of polycrystalline sample, thermalized by ca. 0.2 mg of Apiezon N grease, whose contribution was subtracted by using a phenomenological expression.

Crystallography

Single crystals of suitable dimensions were used for data collection. The intensity data for compounds **1**, **4** and **7** were collected on a Bruker D8 Venture, while for compounds **3**, **5**, **6** and **9** diffraction intensities were collected on a Bruker AXS APEX diffractometer, both equipped with graphite monochromated Mo Kα radiation (λ = 0.7107 Å). For compound **2** diffraction intensities were collected at 100(2) K on an Agilent Technologies Super-Nova diffractometer, which was equipped with monochromated Mo Kα radiation and an Eos CCD detector. For **8**, data were also collected by using an Agilent Technologies Super-Nova diffractometer, but with monochromated Cu Kα radiation (λ = 1.5418 Å) and an Atlas detector.

For **2** and **8**, data frames were processed (unit cell determinations, intensity data integrations, routine corrections for Lorentz and polarization effects and analytical absorption corrections) using the CrysAlis Pro software package.[14] For the rest of the compounds the data reduction was performed with the APEX2 software[15] and corrected for absorption using SADABS.[16]

The structures were solved by direct methods and refined by full-matrix least-squares with SHELXL-2018.[17] Final *R*(F), *wR*(F^2) and goodness of fit agreement factors, details of the data collection and analysis can be found in Table S1. Selected bond lengths and angles are given in Table S2. CCDC reference numbers for the structures are 1561137-1561144 and 2169104.

The powder X-ray diffraction patterns were collected on a Philips X'PERT diffractometer using Cu Kα radiation (λ = 1.5418 Å) over the range 5 < 2θ < 50° with a step size of 0.026° and an acquisition time of 2.5 s per step at 25 °C.

DFT calculations

DFT calculations on **1**, **4**, **6** and **8** were performed by using the SIESTA (Spanish Initiative for Electronic Simulations with Thousands of Atoms) code[18] together with the PBE functional.[19] Only valence electrons were included in the calculations, with the core being replaced by norm-conserving scalar relativistic pseudopotentials factorized in the Kleinman-Bylander form.[20] The pseudopotentials were generated according to the procedure of Trouiller and Martins.[21] For gadolinium atoms, the pseudopotential and triple-ζ basis set proposed by Pollet *et al*. were used.[22] In complex **1**, bromine atoms were substituted by chlorine atoms.

The *J* values were determined by calculating the energy difference between the high spin state (E_{HS}) and broken symmetry state (E_{BS}), according to the following equation:

$$J = (E_{BS} - E_{HS}) /21 \qquad \text{(Eq. 1)}$$

using the Heisenberg Hamiltonian $\hat{H} = -J\hat{S}_1\hat{S}_2$. $\hat{S}_1$ and $\hat{S}_2$ account for the local spin operators for each metal center.

Results and discussion

The reaction of H_2L^1 with $Mn(OAc)_2$·4H$_2$O and $Ln(NO_3)_3$·nH_2O in acetonitrile/methanol mixture and in 1:1:1 molar ratio allows the formation of di-μ-phenoxido/*syn-syn* acetate triply bridged dinuclear species [Mn(μ-L^1)(μ-OAc)Gd(NO$_3$)$_2$]·CH$_3$CN·H$_2$O (**1**) and [Mn(μ-L^1)(μ-OAc)Dy(NO$_3$)$_2$]·CH$_3$CN·H$_2$O (**2**) (Fig. 1). The reaction of H_2L^2 with $Mn(NO_3)_2$·4H$_2$O and $Dy(NO_3)_3$·5H$_2$O in MeOH and in 1:1:1 ratio led to crystals of complex [Mn(CH$_3$OH)(μ-L^2)Dy(NO$_3$)$_3$] (**3**). The same reaction but using $Mn(OAc)_2$·4H$_2$O instead of $Mn(NO_3)_2$·4H$_2$O and the appropriated lanthanide salt led to the two dinuclear complexes [Mn(μ-L^2)(μ-OAc)Gd(NO$_3$)$_2$] (**4**) and [Mn(μ-L^2)(μ-OAc)Dy(NO$_3$)$_2$] (**5**), where the Mn(II) and Ln(III) ions are bridged by the two phenoxido groups of the ligand and an acetate bridge. The acetate bridge could be replaced by 9-anthracenecarboxylate in complexes [Mn(μ-L^2)(μ-9-An)Gd(NO$_3$)$_2$]·2CH$_3$CN (**6**) and [Mn(μ-L^2)(μ-9-An)Dy(NO$_3$)$_2$]·2CH$_3$CN (**7**) by reacting an acetonitrile solution containing H_2L^2, $Mn(NO_3)_2$·4H$_2$O and the corresponding $Ln(NO_3)_3$·nH_2O (1:1:1 molar ratio) with another acetonitrile solution containing 9-anthracene
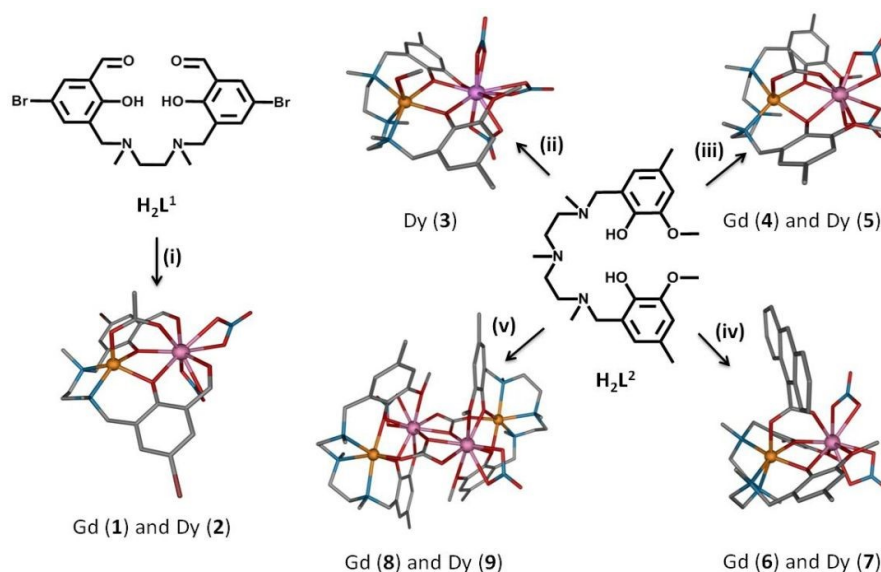
Fig. 1.- (i) H_2L^1/Mn(OAc)$_2$·4H$_2$O/ Ln(NO$_3$)$_3$·nH$_2$O, 1:1:1 in CH$_3$CN/MeOH (Ln = Gd (**1**), Dy (**2**)). (ii) H_2L^2/Mn(NO$_3$)$_2$·4H$_2$O/Dy(NO$_3$)$_3$·5H$_2$O, 1:1:1 in MeOH (**3**). (iii) H_2L^2/Mn(OAc)$_2$·4H$_2$O/Ln(NO$_3$)$_3$·nH$_2$O, 1:1:1 in MeOH (Ln =Gd (**4**), Dy (**5**)). (iv) H_2L^2/Mn(NO$_3$)$_2$·4H$_2$O/Ln(NO$_3$)$_3$·nH$_2$O/H$_2$-9-An/Et$_3$N, 1:1:1:1:1 in CH$_3$CN (Ln = Gd (**6**), Dy (**7**)). (v) H_2L^2/Mn(NO$_3$)$_2$·4H$_2$O/Ln(NO$_3$)$_3$·nH$_2$O/Et$_3$N/Na$_2$CO$_3$, 1:1:1:2:1 in CH$_3$OH/H$_2$O (Ln = Dy (**8**), Gd (**9**)). Hydrogen atoms are omitted for the sake of clarity. Colour code: N = blue, O = red, C = gray, Br = brown, Mn = orange, Ln = pink.

carboxylic acid and Et$_3$N (1:1 molar ratio). To end up, the tetrameric complexes {(μ_3-CO$_3$)$_2$[Mn(μ-L^2)Gd(NO$_3$)]$_2$}·(CH$_3$OH)$_2$·H$_2$O (**8**) and {(μ_3-CO$_3$)$_2$[Mn(μ-L^2)Dy(NO$_3$)]$_2$}·(CH$_3$OH)$_2$ (**9**) were obtained by reacting H$_2$L^2, Mn(NO$_3$)$_2$·4H$_2$O, the corresponding Ln(NO$_3$)$_3$·nH$_2$O and Et$_3$N (1:1:1:2 molar ratio) in methanol with an aqueous solution of an equimolar amount of sodium carbonate.

Crystal structures

Complexes **1** and **2** crystallize in the P2$_1$/n space group and consist on di-μ-phenoxido/acetate triply bridged Mn(II)Ln(III) complexes based on the ligand H$_2$L^1 (Fig. 1 and S5). The fully deprotonated (L^1)$^{2-}$ ligand adopts a 2κ-O$_{1A}$, 1κ-O$_{2A}$:2κ-O$_{2A}$, 1κ^2-N,N', 1κ-O$_{3A}$:2κ-O$_{3A}$, 2κ-O$_{4A}$ hexadentate coordination mode in these complexes (O$_{2A}$ and O$_{3A}$: phenoxido oxygen atoms, O$_{1A}$ and O$_{4A}$ aldehyde oxygen atoms), where the Mn(II) ions are in the inner site coordinated to four of the heteroatoms of the ligand. The MnN$_2$O$_3$ coordination spheres are formed by further coordination to an oxygen atom of a *syn-syn* acetate group and can be considered as square pyramids according to the continuous shape measure theory and SHAPE software (Table S3).[23] The Mn-O and Mn-N distances are found in the 2.053(2)-2.148(2) and 2.220(2)-2.230(2) Å ranges, respectively; the shortest Mn-O distance corresponds to the Mn-O$_{acetate}$ bond. The Ln(III) ions lie in the outer coordination site of the ligand and, in addition to the four oxygen atoms of the ligand (two phenoxido and two aldehyde), they are coordinated by two bidentate nitrate anions and by an oxygen atom belonging to the *syn-syn* acetate group. The calculation of the degree of distortion of the Ln(III) coordination polyhedron with respect to the ideal nine-vertex polyhedral, by using the SHAPE software (Table S5), indicates that the LnO$_9$ coordination sphere can be considered intermediate between several reference ideal

polyhedra, but close to an spherical capped square antiprism. The Ln-O bond distances are in the 2.295(2)-2.525(2) Å range, the shortest ones corresponding to the Ln-O$_{acetate}$ bond, while the largest ones are those involving the Ln-O$_{nitrate}$ bonds.

The average Mn-O-Ln angles are of 97.53 and 97.72° respectively for **1** and **2**, while the average hinge angles of the Mn-(μ-O)$_2$-Ln bridging fragment is of 34.85 and 34.86°, respectively. These complexes exhibit hydrogen bond interactions between the crystallization acetonitrile and water molecules, with donor-acceptor distances of 2.986(9) and 3.022(9) Å for **1** and **2**, respectively (Fig. S6). Bond lengths and angles for **1** and **2** and the rest of the complexes can be found in Supporting Information (Table S2), together with SHAPE measurement results (Tables S3-S6).

Complex **3** also crystallizes in the *P2$_1$/n* space group and is isostructural to the Mn(II)Gd(III) complex previously reported by some of us in 2013.[24] Its molecular structure consists of dinuclear molecules in which the Mn(II) and Dy(III) ions are bridged by two phenoxido groups of the (L^2)$^{2-}$ ligand (Fig. 1 and S7). Besides the two phenoxido bridging oxygen atoms, the MnN$_3$O$_3$ coordination polyhedron is formed by three nitrogen atoms from the amine groups of the ligand and one oxygen atom belonging to a methanol molecule. Therefore, the ligand H$_2$L^2 acts in a 2κ-O$_{1A}$, 1κ-O$_{2A}$:2κ-O$_{2A}$, 1κ^3-N,N',N'', 1κ-O$_{3A}$:2κ-O$_{3A}$, 2κ-O$_{4A}$ bridging mode (O$_{2A}$ and O$_{3A}$: phenoxido oxygen atoms, O$_{1A}$ and O$_{4A}$ methoxo oxygen atoms). The three oxygen atoms and, consequently, the three nitrogen atoms occupy *fac* positions in the trigonally distorted coordination polyhedron, which shows continuous shapes measures (CshM) values of 5.541 and 6.579 respectively for trigonal prism and octahedron ideal geometries (Table S4). The Mn-O and Mn-N

Journal Name

ARTICLE

distances are found in the 2.146(3)-2.217(3) and 2.295(4)-2.377(3) Å ranges, respectively.

The DyO_{10} coordination sphere is made of two phenoxido bridging oxygen atoms, two methoxo oxygen atoms and six oxygen atoms belonging to three bidentate nitrate anions. The DyO_{10} coordination sphere is rather unsymmetrical, exhibiting short Dy-$O_{phenoxido}$ distances of 2.291(3) and 2.312(3) Å, long Dy-$O_{methoxo}$ distances of 2.556(3) and 2.611(3) Å and intermediate Dy-$O_{nitrate}$ distances (in the 2.464(3)-2.517(3) Å range). The use of the continuous shape measure theory and SHAPE software indicates that the DyO_{10} coordination sphere is intermediate between several ten-vertex polyhedral but close to a sphenocorona (Table S6).

The Mn-$(\mu$-O$)_2$-Dy bridging fragment is almost planar with a hinge angle of 4.49° and rather symmetric, with similar pairs of Mn-O bond distances (2.146(3) Å and 2.152(3) Å), Dy-O bond distances (2.291(3) Å and 2.312(3) Å) and Mn-O-Dy bridging angles (110.36(11) and 110.93(11)°). To end up with **3**, it should be stressed out that in this complex, the molecules are held together in pairs by a couple of symmetrically related intermolecular hydrogen bonds involving the non-coordinated O atom of one of the bidentate nitrate anions and the methanol molecule, with O···O distances of 2.829 Å (Fig. S8).

The structures of complexes **4** and **5** are given in Fig. 1 and S9, where the most significant change compared to **3** is the substitution of the coordinated methanol and one of the bidentate nitrate molecules for a bridging acetate group. As expected, the incorporation of a third bridging fragment forces the structures to be folded with higher hinge angles (23.27° for **4** and 23.72° for **5**), which leads to a decrease in the average Mn-O-Ln angles (101.94° for **4** and 102.07° for **5**). The acetate bridge also affects the MnN_3O_3 coordination spheres, leading to octahedral coordination environments according to SHAPE measurement results (Supporting Information, Table S4) and reduces to 9 the number of oxygen atoms coordinated to the lanthanide atoms. These complexes are entirely devoid of hydrogen bonds.

The structures of complexes **6** and **7** are shown in Fig. 1 and S10 and are very similar to those of complexes **4** and **5** but with a 9-anthracenecarboxylate bridging ligand instead of an acetate ligand connecting the Mn(II) and Ln(III) ions, and with two crystallization acetonitrile molecules. Compared to the acetate bridged analogues, complexes **6** and **7** exhibit similar bond lengths, accompanied with slightly smaller hinge angles (20.74° for **6** and 20.72° for **7**).

Finally, complexes **8** and **9** consist in centrosymmetric tetranuclear compounds, which are made by two cationic $[Mn(\mu$-$L^2)Ln(NO_3)]^{2+}$ units connected by two tetradentate carbonate bridging ligands acting in a μ_3-κ^2-O,O':κ-O:κ-O" coordination mode (Fig. 1 and S11). The Mn(II) ions show similar coordination environments to those of complexes **4**-**7**, but they are coordinated to a carbonate bridging ligand instead of to an acetate or anthracenate bridging ligands. The lanthanide ions exhibit rather unsymmetric LnO_9 coordination spheres, which are made by the two phenoxido bridging oxygen atoms, the two methoxo oxygen atoms, three oxygen atoms from the carbonate bridging groups and two oxygen atoms belonging to a bidentate nitrate anion. The Ln-O distances are in the 2.300(4)-2.571(5) and 2.266(4)-2.567(4) Å range for **8** and **9**, respectively. In these complexes, the LnO_9 coordination spheres can be considered
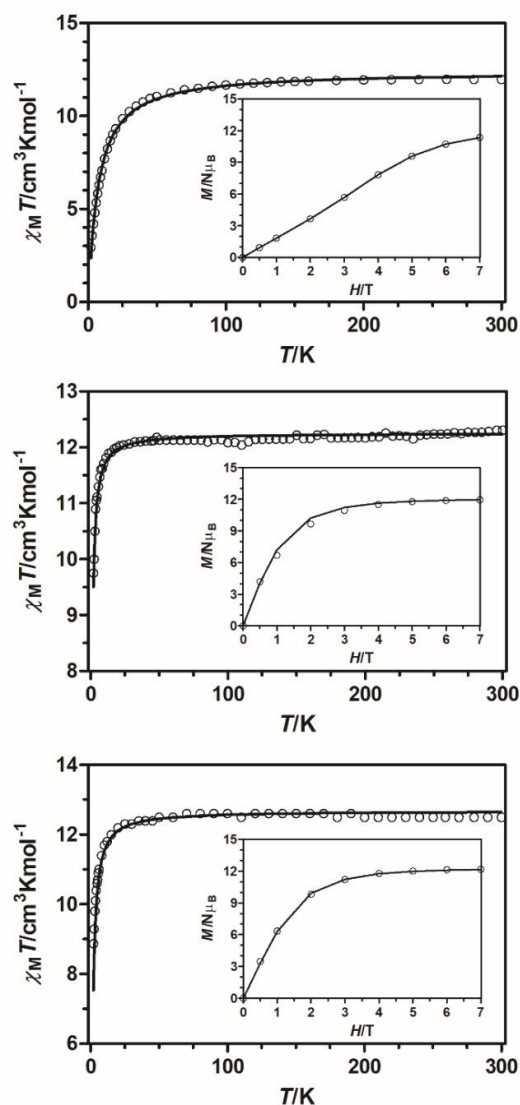
Fig. 2.- Temperature dependence of the $\chi_M T$ product for **1** (top), **4** (middle) and **6** (bottom). Insets: field dependence of the magnetization. The solid lines are generated from the best fit to the magnetic parameters.

as intermediate between several reference ideal polyhedron, the closest ideal geometry according to SHAPE measurements being muffin (MFF-9) (Supporting Information, Table S5). To end up, the Mn-$(\mu$-O$)_2$-Ln bridging fragments show smaller hinge angles than in complexes **4**-**7**, being of 14.42° for **8** and of 13.34° for **9**, whereas the Ln-$(\mu$-O$)_2$-Ln bridging fragments are planar.

Magnetic properties

The temperature dependence of the $\chi_M T$ products (χ_M being the molar paramagnetic susceptibility of the compound) for the reported complexes were measured on polycrystalline samples under an applied magnetic field of 0.1 T and are represented in Fig. 2, 3, S12 and S13.

Journal Name ARTICLE

Starting with the dinuclear Mn(II)Gd(III) complexes **1**, **4** and **6**, the room temperature $\chi_M T$ values of 11.97, 12.31 and 12.50 cm³·K·mol⁻¹ are in agreement with the expected value for a pair of non-interacting Mn(II) ($S = 5/2$) and Gd(III) ($S = 7/2$) ions with $g = 2$ (12.25 cm³·K·mol⁻¹). On lowering the temperature, the $\chi_M T$ product for **1** decreases first gradually and below approximately 50 K in a sharper manner to reach a value of 2.93 cm³·K·mol⁻¹ at 2 K. The $\chi_M T$ product for **4** and **6** remains almost constant until approximately 25 K and then drops abruptly to reach values of 9.75 and 8.87 cm³·K·mol⁻¹ at 2 K for **4** and **6**, respectively. The observed behaviour is due to weak antiferromagnetic (AF) interactions within the dinuclear units, which are stronger in the case of **1**. The field dependence of the magnetization at 2 K for **1** shows a sigmoidal shape reaching a value of 11.34 Nμ_B at 7 T (Fig. 2, inset). This value is lower than the expected value for non-interacting Gd(III) ($S = 7/2$) and Mn(II) ($S = 5/2$) ions of 12 Nμ_B. This fact, together with the lack of saturation at the maximum applied field indicates the existence of weak AF interactions. On the other hand, complexes **4** and **6** show a relatively rapid increase in the magnetization at low fields and a rapid saturation that is almost complete above 4 T, reaching a value of 11.96 and 12.19 Nμ_B at 7 T, respectively. These results clearly indicate that the AF interaction in complexes **4** and **6** is so small that the magnetization value at 7 T is close to the value expected for non-interacting atoms. Therefore, the field dependence of the magnetization supports the presence of weak AF interactions in **1** that are stronger than those observed for **4** and **6**.

The magnetic data for complexes **1**, **4** and **6** have been modelled by using the PHI program[25] and the following spin-Hamiltonian:

$$H = -JS_{Mn}S_{Gd} + g\mu_B S_{Mn}B + g\mu_B S_{Gd}B \quad \text{(Eq. 2)}$$

where the first term accounts for the isotropic magnetic exchange coupling between the Mn(II) and Gd(III) ions and the last two terms correspond to the Zeeman interaction (g has been considered to be equal for both atoms). The susceptibility and magnetization data were simultaneously fitted to the above Hamiltonian, affording the following set of parameters, $J = -0.82$ cm⁻¹ and $g = 2.00$ with $R = 1.8 \cdot 10^{-4}$ for **1**, $J = -0.08$ cm⁻¹ and $g = 2.00$ with $R = 3.7 \cdot 10^{-5}$ for **4** and $J = -0.16$ cm⁻¹ and $g = 2.03$ with $R = 5.8 \cdot 10^{-5}$ for **6**. The obtained experimental exchange coupling constants were supported by DFT calculations on the X-ray structures, which led to the calculated J values that are collected in Table 1.

The unsolvated tetranuclear complex **8** shows a value of 24.9 cm³·K·mol⁻¹ at 300 K (solvent molecules are not considered in the molecular weight), which agrees well with the expected value for the sum of two Mn(II) and two Gd(III) ions with $g = 2.0$ (24.5 cm³·K·mol⁻¹). Upon cooling, this value remains constant until 30 K and then starts decreasing to reach a value of 15.7 cm³·K·mol⁻¹ at 2 K (Fig. 3), which suggests the presence of weak overall AF interactions in the molecule. The magnetization plot for **8**, with a relatively rapid increase in the magnetization at low fields and a rapid saturation that is almost complete above 4 T, shows a saturation value of 24.07 Nμ_B at 7 T, which is in good agreement with the theoretical value expected for two Mn(II) and two Gd(III) non-interacting atoms (24 Nμ_B for $g = 2.0$). The magnetic susceptibility and magnetization data of **8** were simultaneously fitted using the following Hamiltonian:
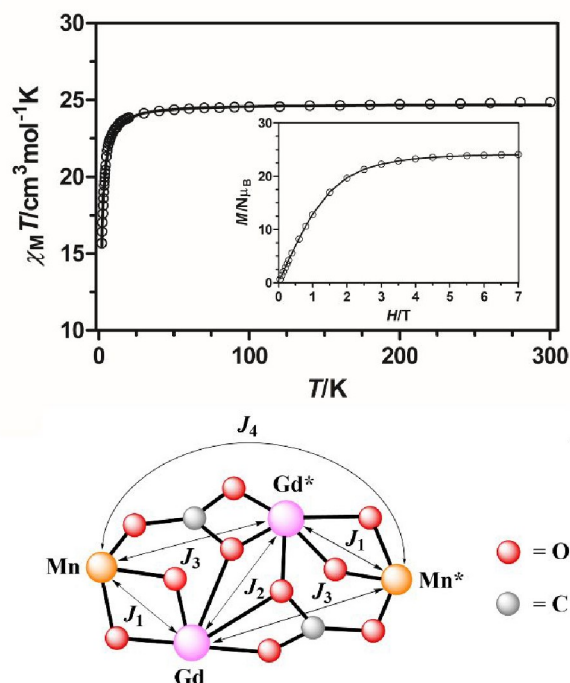
Fig. 3.- Top: Temperature dependence of the $\chi_M T$ product for **8**. Inset: field dependence of the magnetization for **8**. The solid lines are generated from the best fit to the magnetic parameters. Bottom: Magnetic exchange pathways in compound **8**.

$$H = -J_1(S_{Mn}S_{Gd} + S_{Mn*}S_{Gd*}) - J_2 S_{Gd}S_{Gd*} - J_3$$
$$(S_{Mn}S_{Gd*} + S_{Mn*}S_{Gd}) - J_4 S_{Mn}S_{Mn*} + g\mu_B(S_{Mn} + S_{Mn*})B + g\mu_B$$
$$(S_{Gd} + S_{Gd*})B \quad \text{(Eq. 3)}$$

where J_1, J_2, J_3 and J_4 account for the exchange pathways described in Fig. 3. In order to avoid overparametrization, the exchange pathways J_3 and J_4, where the metal ions are quite far from each other (at distances of 5.552(2) and 8.355(3) Å for pathways 3 and 4, respectively), were not considered. The best fit parameters after fixing g to 2.01 for all ions were $J_1 = -0.17$ cm⁻¹ and $J_2 = +0.05$ cm⁻¹, with $R = 4.6 \cdot 10^{-5}$. The obtained results suggest the presence of very weak AF interactions between the di-μ-phenoxido/carboxylate triply bridged Mn(II) and Gd(III) ions, combined with very weak F interactions between Gd(III) ions. DFT calculations carried out on the X-ray structure support the experimentally obtained values, with $J_1 = -0.065$ cm⁻¹ and $J_2 = +0.12$ cm⁻¹ and allow us to know that the exchange coupling through pathways 3 and 4 are ferromagnetic (F) in nature, with $J_3 = +0.10$ cm⁻¹ and $J_4 = +0.062$ cm⁻¹. Although all the coupling constants are very weak, it seems that AF interactions are dominant, as the overall interaction is AF in nature.

Regarding the Dy(III) based derivatives, the $\chi_M T$ values at 300 K of 18.50, 18.89, 18.36 and 18.80 cm³·K·mol⁻¹, respectively for the Mn(II)Dy(III) dinuclear complexes **2**, **3**, **5** and **7** (Fig. S12 and S13), are close to the expected value for a pair of non-interacting Mn(II) ($S = 5/2$, $g = 2$) and Dy(III) (4f⁹, $J = 15/2$, $S = 5/2$, $L = 5$, $g = 4/3$ ⁶H$_{15/2}$) ions

Dalton Transactions

Journal Name ARTICLE

Table 1.- Magneto-structural data for polynuclear Mn(II)$_x$Gd(III) (x = 1, 2) complexes and complexes reported in this work.

Complex	J_{exp}/J_{calc} (cm^{-1})[a]	N° of bridges	θ (°)[b]	β (°)[c]	Mn···Gd (Å)	Ref.
[MnGd{pyCO(OEt)pyC(OH)(OEt)py}$_3$](ClO$_4$)$_2$	-1.7/-2.7	3	87.61	55.1	3.125	26
[Mn(CH$_3$OH)(μ-L^2)Gd(NO$_3$)$_3$]	+0.99/+1.27[d]	2	110.48	4.06	3.686	24
[Mn(μ-L^1)(μ-OAc)Gd(NO$_3$)$_2$]·CH$_3$CN·H$_2$O (**1**)	-0.82/-2.22	3	97.53	34.85	3.414	T.w.
[Mn(μ-L^2)(μ-OAc)Gd(NO$_3$)$_2$] (**4**)	-0.08/-0.61	3	101.94	23.27	3.474	T.w.
[Mn(μ-L^2)(μ-9-An)Gd(NO$_3$)$_2$]·2CH$_3$CN (**6**)	-0.16/-0.32	3	103.2	20.74	3.485	T.w.
{(μ$_3$-CO$_3$)$_2$[Mn(μ-L^2)Gd(NO$_3$)]$_2$} (**8**)	-0.17/-0.065	3	102.2	14.42	3.522	T.w.
	+0.10 (calc.)	1	-	-	5.552	
[L^{3}Mn(H$_2$O)$_2$]$_2$[Gd(NO$_3$)$_5$(MeOH)]	e	3	93.32	50.71	3.312	27
[(NO$_3$)Mn$_2$(L^4)$_2$(μ-NO$_3$)Gd](NO$_3$)	+0.0/-0.2	3	101.2	39.8	3.515	28
	+1.6/+1.9	2	102.4	3.3	3.709	
[L^{5}MnGdMnL^5]NO$_3$	+0.08 (exp)	3	93.76	50.33	3.334	29
		3	93.75	50.32	3.335	

[a] J_{MnGd}. [b] Average Mn-O-Ln angles. [c] Average hinge angles of the Mn-(μ-O)$_2$-Ln bridging fragments. [d] Calculated after article publication.
[e] Overall ferromagnetic exchange coupling observed, exchange constants are not obtained. T.w. = this work.
H$_2$L^3 = 1,3-bis((methoxysalicylidene)amino)-2,2'-dimethylpropane)
H$_2$L^4 = N,N'-2,2-dimethylpropylenebis(3-methoxysalicylideneimine)
H$_2$L^5 = N,N',N''-tris(2-hydroxy-3-methoxybenzilidene)-2-(aminomethyl)-2-methyl-1,3-propanedi-amine

(18.55 cm^3·K·mol^{-1}). On cooling, the $\chi_M T$ product for **2** decreases slowly until 100 K and then in a more abrupt way, reaching a value of 7.82 cm^3·K·mol^{-1} at 4.5 K. This behaviour is essentially due to the depopulation of the M_J sublevels of the Dy(III), which arises from the splitting of the ground term by the crystal field. In order to determine the nature of the magnetic interaction between Mn(II) and Dy(III) ions, the contribution of the crystal-field effects of the Dy(III) ion was removed by subtracting from the experimental $\chi_M T$ data of **2** those of the isostructural complex Zn(II)Dy(III).[30] The difference $\Delta\chi_M T$ = $(\chi_M T)_{MnDy}$ - $(\chi_M T)_{ZnDy}$ indicates the nature of the overall exchange interaction between the Mn(II) and Dy(III) ions. Thus, positive and negative values indicate F and AF couplings, respectively. The $\Delta\chi_M T$ value is almost constant over the whole temperature range (Fig. S14), except for a decrease in the lowest-temperature region to reach negative values below 11 K, thus indicating AF interaction between Mn(II) and Dy(III) ions. On the other hand, the $\chi_M T$ products for **5** and **7** stop decreasing in the lowest temperatures region, remaining almost constant below 8 K in the case of **5** and showing a slight increase below 16 K in the case of **7**, which could be due in both cases to the presence of very weak F interactions between the metal ions. The F interaction is more pronounced in complex **3**, where the $\chi_M T$ product increases below 35 K to reach a maximum at 5 K (24.23 cm^3·K·mol^{-1}) and then drops to 23.65 cm^3·K·mol^{-1} at 2.5 K probably due to intermolecular interactions. The obtained results are not surprising, as the isostructural Gd(III) based complex reported by some of us[24] exhibits, as far as we know, the strongest F interaction ever observed for a Mn(II)Gd(III) dinuclear complex (J = + 0.99 cm^{-1}). The magnetization plots of complexes **3**, **5** and **7** (Fig. S12 and S13, insets) show a relatively rapid increase in the magnetization at low fields and a rapid saturation of the magnetization, reaching values of

9.77, 9.79 and 9.87 Nμ_B at 5 T, respectively. In the case of complex **2**, the magnetization curves exhibit a slower increase, which is probably due to the AF interactions that are expected for this complex. The obtained value of 9.25 Nμ_B at 5 T is lower than the expected value of 17 Nμ_B ($M_J = g_J N\mu_B$) for a Mn(II)Dy(III) pair, which, as in the case of complexes **3**, **5** and **7**, is due to crystal field effects of the Dy(III) ion, leading to magnetic anisotropy, and also to possible AF interactions in the case of **2**.

Finally, the room-temperature $\chi_M T$ value for the tetranuclear complex **9** is 37.31 cm^{3}Kmol^{-1} (solvent molecules are not considered in the molecular weight), which is consistent with the theoretical value expected for the sum of two Mn(II) and two Dy(III) ions (37.60 cm^3·K·mol^{-1}). On lowering the temperature, the $\chi_M T$ starts decreasing at around 150 K to reach a minimum value of 34.06 cm^3·K·mol^{-1} at 14 K, whereupon increases until 36.73 cm^3·K·mol^{-1} at 2 K. The increase at low temperatures suggests the presence of overall F interactions, while the observed decrease at high temperatures is due to the crystal field splitting effects of the Dy(III) ions. As in the previous Dy(III) based complexes, the magnetization saturation value at 2 K (25.3 Nμ_B) is lower than the expected value (34 Nμ_B), which is also due to the anisotropy of the Dy(III) ions.

In order to analyze the magnetic data of the Mn(II)Dy(III) dinuclear complexes (the analysis of the tetranuclear compound **9** could not be carried out because of the large dimension of the matrices), we have followed two approaches recently proposed by Herchel and coworkers.[31] The first one uses the following Hamiltonian:

$$\hat{H} = -J\hat{S}_{Mn}\hat{J}_{Dy} + D_{Ln}\left(\hat{J}_{zDy}^2 - \frac{1}{3}J(J+1)\right) + E_{Dy}\left(\hat{J}_x^2 - \hat{J}_y^2\right) + \mu_B\vec{B}(\overline{\overline{g}}_{Mn}\vec{S}_{Mn} + \overline{\overline{g}}_{Dy}\hat{J}_{Dy})$$ (Eq. 4)

In this method the ground multiplet of the Dy(III) is described in the |JM> basis, where D_{Dy} and E_{Dy} define the zero-field splitting and $\hat{J}_{Dy}$,

Please do not adjust margins

Dalton Transactions

Page 8 of 13

View Article Online
DOI: 10.1039/D2DT01869A

Journal Name

ARTICLE

$\hat{J}^2_{zDy}$ and J represent the total angular momentum operator, its z component and the quantum number, respectively. The exchange coupling is defined between the pseudo-spin $J_{Dy} = 15/2$ and $S_{Mn} = 5/2$. The simultaneous fitting of the susceptibility and magnetization afforded the parameters given on Table S7.

The second approach uses the |LS> basis for the Dy(III), so that the exchange interaction is defined between true spins. The corresponding Hamiltonian is as follows:

$$\hat{H} = -J\hat{S}_{Mn}\hat{S}_{Dy} + \sum_{j=1}^{2SLn}\lambda_j(\sigma\hat{L}_{Dy}\hat{S}_{Dy}) + \sigma D_{Ln}\left(\hat{L}^2_{zDy} - \frac{1}{3}L(L+1)\right) +$$
$$\sigma E_{Dy}\left(\hat{L}^2_x - \hat{L}^2_y\right) + \mu_B\vec{B}(\overline{\overline{g}}_{Mn}\vec{S}_{Mn} + \overline{\overline{g}}_{Dy}\vec{S}_{Dy} + \sigma\vec{L}_{Dy}) \quad \text{(Eq. 5)}$$

where the λ_{Dy} spin-orbit coupling parameter and the $g_{L,Dy}$ and $g_{S,Dy}$ were set by default in the PHI software.[25] σ is the orbital reduction factor that takes into account the covalency and D_{Ln} and E_{Ln} are parameters that act on the angular momentum ($D = 3B^0_2\theta_2$ and $= B^2_2\theta_2$). The best fit of the magnetic data led to the parameters indicated on Table S7.

It should be noted that the low sensitivity of the magnetic measurements for determining D and E parameters, together with the limitations of these approaches, lead to unconfident values of these parameters, particularly the sign and magnitude of E and the sign of D. Therefore, the D values extracted from the dc magnetic measurements for these complexes, should be taken with some prudence. However, for the magnetic exchange coupling J parameters, rather confident values are extracted. It is worth to mention that the J value extracted from both methods are very similar. Moreover, the magnitude of the interactions follow the same order as for the isostructural Mn(II)Gd(III) complexes, because compound **5** and **7**, with J values in the ranges 0.46-0.48 cm^{-1} and 0.16-0.18 cm^{-1}, respectively, exhibit weaker interactions than **2** and **3**, with J values in the ranges -0.84-(-0.90) cm^{-1} and 1.46-1.52 cm^{-1}, respectively.

Magneto structural correlations

DFT calculations and experimental results[32] have clearly shown that the AF J_{MGd} coupling in di-μ-phenoxido bridged M(II)-Gd(III) complexes (M = Mn, Ni, Cu) decreases when the planarity of the M-(μ-O)$_2$-Gd bridging fragment (β) and the M-O-Gd bridging angle (θ) increase. Both structural factors are correlated, so that the latter increases as the bridging fragment becomes more planar.

As far as we know, Table 1 collects the magneto-structual data reported so far for the dinuclear Mn(II)Gd(III) and trinuclear Mn(II)Gd(III)Mn(II) complexes. In general, it can be said that the highest F coupling constants are shown by double di-μ-phenoxido bridged complexes, which show the lowest hinge angles accompanied with high θ angles, in agreement with the above considerations. The incorporation of a third bridge to di-μ-phenoxido bridged species leads to more folded structures, which consequently exhibit smaller Mn-O-Gd angles than the planar fragments. If the third bridge is a phenoxido bridge, the magnetic exchange decreases but continues being F as in the case of complexes [L^{3}Mn(H$_2$O)$_2$]$_2$[Gd(NO$_3$)$_5$(MeOH)][27] and [L^{5}MnGdMnL^5]NO$_3$.[29] On the other hand, the incorporation of carboxylate and nitrate bridges leads to complexes with very weak AF interactions, as seen in the four complexes reported in this work and in complex
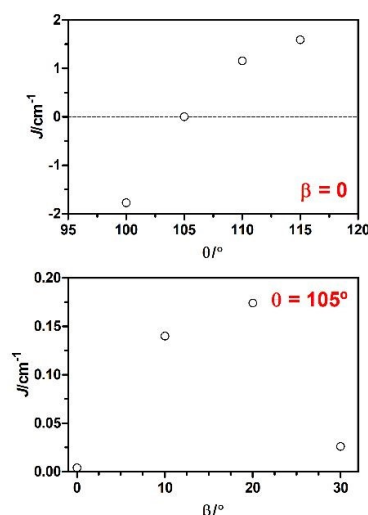
Fig. 4.- J_{MnGd} versus θ (top) and β (bottom) plots for the model compound [Mn(PMTA)(H$_2$O)(μ-OPh)$_2$Gd(OCH$_3$)$_2$(H$_2$O)(NO$_3$)$_2$)].

[(NO$_3$)Mn$_2$(L^4)$_2$(μ-NO$_3$)Gd](NO$_3$).[28] In connection with this, DFT calculations were carried out on a model compound of **6**, where the anthracenate bridge was replaced by two non-bridging water molecules, without modifying the remainder of the structure. The calculated coupling constant value increased from - 0.32 to + 0.052 cm^{-1}, underlining that in addition to the hinge angle, the nature of the carboxylate bridge has a significant role in decreasing the magnetic exchange coupling. In fact, syn-syn carboxylate bridges are known for transmitting AF interactions. To end up, the triply alkoxo bridged compound [MnGd{pyCO(OEt)pyC(OH)(OEt)py}$_3$](ClO$_4$)$_2$ shows the strongest AF coupling, which is consistent with the fact that this complex has the highest β and lowest θ angles.[26]

However, the complexes reported in Table 1 show a rich structural diversity and more specific magneto-structural correlations should be done. With this in mind, DFT calculations were performed on the model compound [Mn(PMTA)(H$_2$O)(μ-OPh)$_2$Gd(OCH$_3$)$_2$(H$_2$O)(NO$_3$)$_2$)] (where PMTA = 1,1,4,7,7-pentamethyldiethylenetriamine and OPh$^-$ = 4-methylphenolato anion), in which the part of ligand containing the amino nitrogen atoms were replaced by PMTA, the phenoxido-bridging parts of the ligand by 4-methylphenolato bridging groups and the methoxo groups coordinated to the Gd(III) ion by methanol molecules. In addition, the acetate or anthracenate bridging groups were replaced by two non-bridging water molecules, leading to a di-μ-phenoxido bridged simplified model compound (Fig. S15). In the calculations, the hinge angle β was first fixed to zero (planar Mn-(μ-O)$_2$-Gd bridging fragment) and the θ angle was varied in the 100 - 115° range. Fig. 4 shows that for planar bridging fragments the crossover point (point in which the magnetic interaction changes from AF to F) is located at around 105°, being the exchange coupling F at higher angles. On the other hand, to know how the folding of the structure affects J_{MnGd}, the θ angle was fixed to 105° and β was varied between 0 and 30°. The results show F interactions for all the β angles considered, with an increase in J_{MnGd} with increasing β until around 20° and a decrease in J_{MnGd} from that point on (Fig. 4). The

variation in J_{MnGd} with β in alkoxo triply bridged Mn(II)Gd(III) compounds was already studied by E. Ruiz *et al*. in 2012,[32] using the model compound $[MnGd\{pyCO(OEt)pyC(OH)(OEt)py\}_3](ClO_4)_2$ (collected in Table 1).[26] They showed that, in the ~35 – 75° β range, the AF contribution increased with the increase of the β angle, which is consistent with our calculations.

The experimental J_{MnGd} value of + 0.99 cm^{-1} obtained for the di-μ-phenoxido doubly bridged complex $[Mn(CH_3OH)(μ-L^2)Gd(NO_3)_3]$,[24] which possesses a hinge angle of 4.06° and a θ of 110.48°, is consistent with the above calculations. In addition, there exists a linear relationship (with r^2 = 0.96) between the θ angles and experimental *J* values obtained for this complex and the four di-μ-phenoxido/carboxylate triply bridged MnGd complexes prepared from ligands H_2L^1 and H_2L^2 reported in this work (Fig. S16), which exhibit similar structures. These results demonstrate, in good agreement with the DFT calculations (Fig. S16), that the main structural factor governing the nature and sign of the magnetic coupling in di-μ-phenoxido bridged Mn(II)Gd(III) dinuclear complexes is the Mn-O-Gd bridging angle (θ). The difference between experimental and calculated J_{MnGd} is more likely due to the crude model used in the DFT calculations and to limitations inherent to the method.

Noteworthy, it seems that the magneto-structural correlations established for the Mn(II)Gd(III) complexes also apply for the Mn(II)Dy(III) counterparts. Thus, compound **2** exhibits, comparatively, the smallest θ and the biggest β angles among the Mn(II)Dy(III) complexes, and presents the strongest antiferromagnetic interaction, whereas complex **3** having the biggest θ and the smallest β angles shows the strongest ferromagnetic interaction. For **5** and **7**, which show intermediate θ and β angles, weaker magnetic couplings are expected, which, depending on small variation on these angles in the bridging region, can lead either to ferro or antiferromagnetic interactions. In the case of these Mn(II)Dy(III) complexes the interaction is very weakly ferromagnetic, whereas in the isostructural Mn(II)Gd(III) complexes very weakly antiferromagnetic.

Magneto-caloric effect

The magneto-thermal properties of the Mn(II)/Gd(III) complexes **1**, **4**, **6** and **8** have been studied because: (i) the Gd(III) and Mn(II) ions show negligible anisotropy due to the absence of orbital contribution; (ii) the Gd(III) and Mn(II) ions exhibit large single-ion spin (*S* = 7/2 and 5/2, respectively); (iii) the AF interaction between the Gd(III) and Mn(II) ions is very weak, which generates multiple low-lying excited and field-accessible states, each of which can contribute to the magnetic entropy of the system and (iv) the molecules are relatively small with a large metal/ligand mass ratio, thus limiting the amount of passive, non-magnetic elements. All the above factors should favour a large MCE.

The magnetic entropy changes (-ΔS_m) that characterize the magneto-caloric properties of complexes **1**, **4**, **6** and **8** can be calculated from the experimental isothermal field dependent magnetization data (Fig. S17-S19 for **1**, **4** and **6** and Fig. 5 for **8**) by making use of the Maxwell relation:
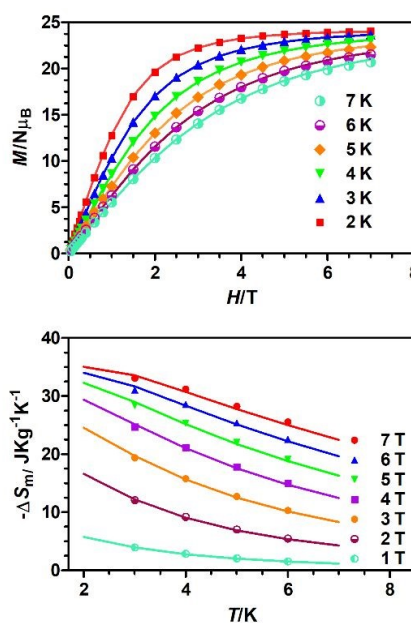
Fig. 5.- Isothermal field dependent curves for **8** between 2 and 7 K (top) and magnetic entropy changes (bottom) simulated with J_1 = - 0.17 cm^{-1}, J_2 = + 0.05 cm^{-1} and *g* = 2.00 between 2 and 7 K (solid lines) and extracted from the experimental magnetization data with the Maxwell equation between 1 to 7 T and temperatures from 3 to 6 K (points).

Table 2.- Maximum magnetic entropy change values (-ΔS_m) at 7 T for complexes **1**, **4**, **6** and **8**, as obtained from magnetization data, and for the Mn(II)Gd(III) complex previously reported by us.[24]

Complex	- ΔS_m (JKg^{-1}K^{-1})	*T* (K)
1	12.5	3
4	27.9	4
6	26.9	3
8	33.1	3
$[Mn(CH_3OH)(μ-L^2)Gd(NO_3)_3]$	23.5	3

$$\Delta S_M = (T, \Delta B) = \int_{B_i}^{B_f} \left[\frac{\partial M(T,B)}{dT} \right]_B dB \qquad \text{(Eq. 6)}$$

where B_i and B_f are the initial and final applied magnetic fields. The integration results show that the values of -ΔS_m for complexes **1**, **6** and **8** under all fields (Fig. S17, S19 and Fig. 5, bottom) increase as the temperature decreases from 7 to 3 K, while for **4** the maximum value is reached at 4 K at 7 T (Fig. S18). The maximum magnetic entropy change values (-ΔS_m) for complexes **1**, **4**, **6** and **8** are given in Table 2.

It should be noted that the -ΔS_m values simulated for complexes **1**, **4**, **6** and **8** at different fields and temperatures using the magnetic parameters (*g* and *J*) extracted from the fitting of the magnetization

ARTICLE
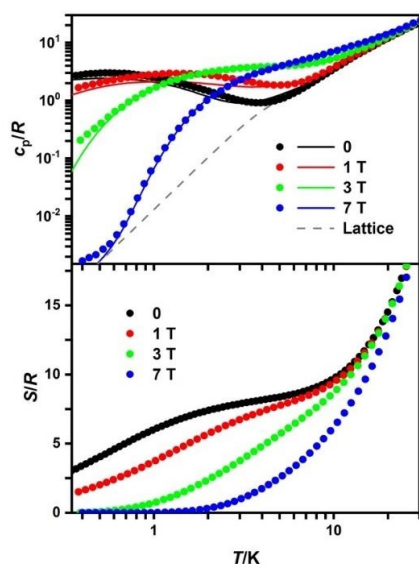
Fig. 6.- Top: Temperature-dependence of the heat capacity c_p, normalized to the gas constant R and measured in the presence of several applied magnetic fields, as labelled. Solid lines correspond to the fits discussed in the text; dashed line is the estimated lattice contribution to the measured heat capacity. Bottom: Experimental entropies as obtained from the corresponding c_p data.

and susceptibility data (Fig. 5 and S17-S19) and the -ΔS_m values extracted from the integration of the field dependence of the magnetization at different temperatures agree rather well, which is a good supporting evidence of the consistency of the MCE values. In the case of the larger tetranuclear complex **8** the -ΔS_m values were further corroborated by temperature-dependent heat capacity (c_p) measurements carried out at applied magnetic fields of up to 7 T (Fig. 6). At high temperatures, the constant increase of experimental c_p is related to vibrational phonon modes of the lattice, which can be fitted with the Debye function (dashed line) affording a Debye temperature θ_D = 26.2 K, which is typical for this class of compounds.[24] At lower temperatures, c_p is dominated by an applied-field sensitive magnetic contribution. The temperature and field dependencies of c_p can be satisfactorily modelled by the sum (solid lines) of the lattice contribution and the Schottky-like heat capacity calculated from the Hamiltonian in Eq. 3 for J_1 = - 0.17 cm^{-1}, J_2 = + 0.05 cm^{-1} and J_3 = J_4 = 0. Fig. 6 bottom displays the temperature dependence of the entropy, which is obtained by the numerical integration of the experimental heat capacity by using Eq. 7:

$$S(T, B) = \int_0^T \frac{c_p(T,B)}{T} dT \qquad \text{(Eq. 7)}$$

The zero-field entropy exhibits a fast increase at the lowest temperatures, reaching a value of ~7.9 R at 3 K (in agreement with the expected saturation value of magnetic entropy, S/R = 2ln(2S_{Mn}+1) + 2ln(2S_{Gd}+1) = 7.74). Above ~8 K, the entropy data increase steadily due to the dominant lattice contribution. The magnetic entropy change, -ΔS_m, is straightforwardly obtained, from Fig. 6, as the difference between the entropy data collected for different applied

fields. Fig. 7 shows that the resulting temperature and applied field dependencies of -ΔS_m agree well with the values estimated from the
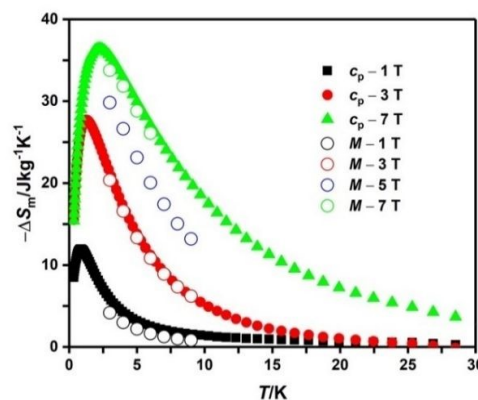
Fig. 7.- Temperature-dependencies of the magnetic entropy change -ΔS_m for compound **8**, for the indicated applied-field changes ΔB, as obtained from heat capacity (full markers) and magnetization (empty markers) measurements.

magnetization data by using the Maxwell relation (Eq. 6), and that -ΔS_m displays the maximum value of 36.4 Jkg^{-1}K^{-1} at ΔB = 7 T and T = 2.2 K. Under these experimental conditions, compound **8** nearly reaches the full magnetic entropy content, i.e., (2Rln(2S_{Gd} + 1) + 2Rln(2S_{Mn} + 1))/M = 7.74 R/M = 41.3 Jkg^{-1}K^{-1} (M = molecular weight) for the desolvated analogue. As far as we know, the maximum experimental value of 36.4 Jkg^{-1}K^{-1} is among the largest -ΔS_m values observed for Mn and Gd based compounds (Table S8).[33]

In the case of the Mn(II)Gd(III) dinuclear complexes, the full magnetic entropy content per mole is (Rln(2S_{Gd} + 1) + Rln(2S_{Mn} + 1))/M = 3.87 R/M, which corresponds to 33.3 Jkg^{-1}K^{-1} for **1**, 38.3 Jkg^{-1}K^{-1} for **4** and 29.7 Jkg^{-1}K^{-1} for **6**. The simulated MCE values at 2 K and 7 T (12.6 Jkg^{-1}K^{-1}, 31.5 Jkg^{-1}K^{-1} and 26.5 Jkg^{-1}K^{-1}, respectively) are rather smaller than their respective full magnetic entropy content, which is mainly due to the AF magnetic coupling between Mn(II) and Gd(III) ions.

From the magnetothermal study of compounds **1**, **4**, **6** and **8** the following conclusions can be drawn:

1.- Regardless of the sign of the magnetic coupling (AF or F interactions), the magnetic entropy changes (-ΔS_m) decrease with increasing the magnetic interaction between Mn(II) and Gd(III) ions (J).

2.- For J values of similar magnitude but opposite sign, as it occurs in compound **1** and [Mn(CH$_3$OH)(μ-L^2)Gd(NO$_3$)$_3$],[24] F interactions between Mn(II) and Gd(III) lead to high values of -ΔS_m. It is worth noting that the magnitude of J has a superior influence on -ΔS_m than F interactions.

3.- Compared to the dinuclear Mn(II)Gd(III) complexes, the tetranuclear Mn$_2$Gd$_2$ complex **8** exhibits enhanced MCE. It is worth noting that even though complexes **4** and **8** exhibit almost the same ligand/metal mass ratio (~0.34 and ~0.37, respectively), however, the MCE is larger for **8**, which could be due to the weak F interaction between the Gd(III) ions through the carbonate bridging groups. Therefore, carbonate ions not only play an important role in connecting dinuclear Mn(II)Gd(III) units, but also induce an enhancement of the MCE. The same explanation has been invoked to justify the increase of MCE on going from a dinuclear Gd$_2$ complex

to the Gd$_4$ complex which is formed by the linking of two Gd$_2$ by carbonato bridging groups.[34]

The results for compounds **4** and **8** clearly show that small clusters based on Mn(II)/Gd(III) coordination compounds can be good aspirant for molecular refrigerants.

Ac magnetic measurements

Alternating-current (*ac*) magnetic susceptibility measurements show that in the absence of an external field, complex **3** shows slightly frequency dependent in-phase (χ_M') and out-of-phase (χ_M'') susceptibility signals (Fig. S20), while the rest of the Dy(III) based compounds do not show any dependency. The *ac* signals of complex **3** can be improved upon an application of an optimal external field of 1000 Oe, which reduces the quantum tunnelling of the magnetization (QTM) (Fig. 8).

The relaxation times for each temperature were extracted from the χ_M'' *vs.* frequency plots and their fit to the Arrhenius equation afforded an effective energy barrier for the reversal of the magnetization of 14.8 K with a τ_0 value of 6.35·10^{-7} s. Although the

Fig. 8.- Temperature dependence of the in-phase χ_M' (top) and out-of phase χ_M'' (middle) components of the *ac* susceptibility for compound **3** under an external field of 1000 Oe. Inset: Arrhenius plot

for the relaxation times of **3**. Bottom: Cole-Cole plots under 1000 Oe external field for **3**. Solid lines represent the best fits to the generalized Debye model.

relaxation times do not deviate significantly from linearity in the 2-4 K range, the Cole-Cole plots, with α values in the 0.31(2 K)-0.03(4 K) range, suggests the existence of multiple relaxation processes at the lowest temperatures (Fig. 8).

To end up, it is worth mentioning that complexes **2**, **5**, **7** and **9** showed a very modest frequency dependency of the in-phase and out-of-phase susceptibility in the presence of an external *dc* field of 1000 Oe (Fig. S21). However, complex **3**, with the strongest F interactions between Mn(II) and Dy(III) ions, is the one that displays the most significant SMM behaviour. This fact seems to support that the increase of the magnetic coupling between an isotropic metal ion and Dy(III) favours the SMMs behaviour.

Conclusions

Nine dinuclear or tetranuclear Mn(II)/Ln(III) complexes (Ln = Gd or Dy) have been prepared using the compartmental ligands N,N'-dimethyl-N,N'-bis(2-hydroxy-3-formyl-5-bromobenzyl)ethylene-diamine (H$_2$L^1) and N,N',N''-trimethyl-N,N''-bis(2-hydroxy-3-methoxy-5-methylbenzyl)diethylenetriamine (H$_2$L^2). The dinuclear Mn(II)Ln(III) complexes have either double di-μ-phenoxido or triple di-μ-phenoxido/carboxylate bridges connecting Mn(II) and Ln(III) ions. In the tetranuclear complexes, two di-μ-phenoxido bridged Mn(II)Ln(III) dinuclear units are linked by two carbonato bridging groups.

Dc magnetic measurements reveal antiferromagnetic exchange interactions between Mn(II) and Gd(III) ions, while ferromagnetic interactions prevail in most of the Mn(II)Dy(III) counterparts. Experimental magneto-structural correlations have been carried out from the Gd(III) based complexes and other complexes found in bibliography, concluding that the highest ferromagnetic coupling constants are observed in di-μ-phenoxido bridged complexes. The observed behaviour has been ascribed to the planarity of the Mn-(μ-O)$_2$-Gd bridging fragment and to the high Mn-O-Gd angles of di-μ-phenoxido bridged complexes, while the incorporation of a third bridge leads to folded structures, reducing the magnetic coupling constant. In addition, DFT calculations carried out in a di-μ-phenoxido doubly bridged model compound show that for planar bridging fragments, the crossover point in Mn-O-Gd angle is located at 105°, being the interactions F above this angle and AF below it. The influence of the Mn-(μ-O)$_2$-Gd hinge angle has also been studied by fixing the Mn-O-Gd angle to 105° and changing the hinge angle, concluding that J_{MnGd} increases when increasing β until around 20° and decreases from that point on. We have estimated the J_{MnDy} coupling constants, and it seems that the magneto-structural correlation established for the Mn(II)Gd(III) complexes also apply for the Mn(II)Dy(III) conterparts.

For the Mn(II)Ln(III) dinuclear complexes, the MCE extracted from the field dependence of the magnetization at different temperatures show that the magnetic entropy changes (-ΔS_m) decrease with increasing the magnetic coupling (either F or AF) between the metal
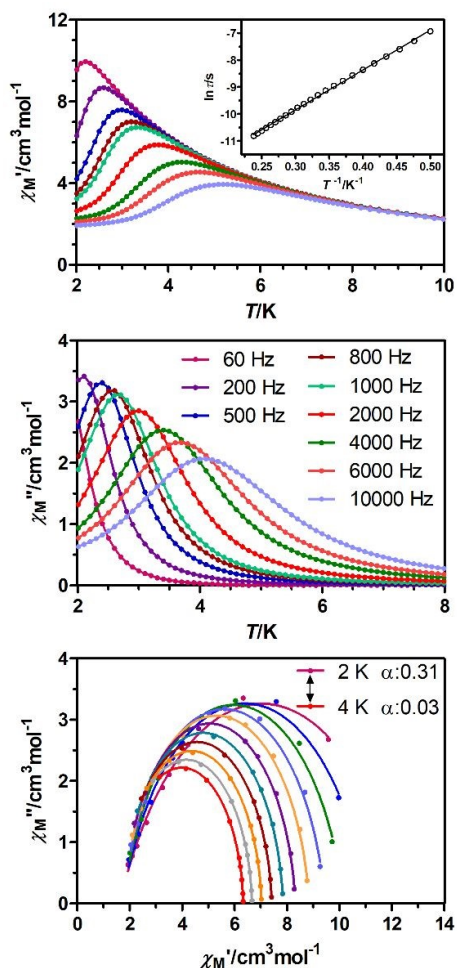
Journal Name

ARTICLE

ions. Nevertheless, ferromagnetic interactions between Mn(II) and Gd(III) lead to higher $-\Delta S_m$ values than the AF ones of similar magnitude. Anyway, the magnitude of J seems to have a superior influence on $-\Delta S_m$ than the ferromagnetic interactions.

For the tetranuclear Mn(II)$_2$Gd(III)$_2$ complex, the relatively low ligand/metal mass ratio and the weak ferromagnetic interaction between the Gd(III) ions through the carbonate bridging groups lead to an enhanced MCE (36.4 Jkg^{-1}K^{-1} at ΔB = 7 T and T = 2.2 K), one of the highest ever observed for Mn(II)/Gd(III) systems. Therefore the connection of Mn(II)Gd(III) dinuclear units with small bridging ligand transmitting ferromagnetic coupling can be a good strategy to enhance MCE.

Finally, complex **3**, with the strongest ferromagnetic interactions between Mn(II) and Dy(III) ions, is the only one that shows significant SMM behaviour, with an energy barrier of 14.8 K under an applied external field of 1000 Oe.

Author Contributions

J.M.S, E.K.B. and E.C. contributed to funding acquisition and supervision. I.O. and A.Z.-L. executed the syntheses. Crystallographic work was carried out by I.O., A.Z.-L. and A.R.-D. Thermogravimetric analysis were performed by A.Z.-L. Elemental analyses measurements were carried out by I.O. Density functional theory studies were performed by A.J.M. Magnetic measurements were conducted and analysed by I.O., M.A.P. and E.C. The magneto-caloric data was collected, simulated and analysed by G.L., M.E. and E.C. After a first complete draft of the manuscript was written by I.O. and E.C., C.R.-E. and A.Z-L. contributed to reviewing and editing the article and all authors gave their consent to its publication.

Conflicts of interest

There are no conflicts to declare.

Acknowledgements

Notes and references

1 R. Sessoli, D. Gatteschi, A. Caneschi and M. A. Novak, *Nature*, 1993, **365**, 141; D. Gatteschi, R. Sessoli and J. Villain, *Molecular Nanomagnets*, Oxford University Press, Oxford, 2006; J. Bartolomé, F. Luis and J. F. Fernández, *Molecular Magnets: Physics and Applications*, Ed. Springer-Verlag, Berlin-Heidelberg, 2014; R. Clérac and R. E. P. Winpenny, *Struct. Bond*., 2016, **172**, 35; L. Escalera-Moreno, J. J. Baldoví, A. Gaita-Ariño and E. Coronado, *Chem. Sci*., 2018, **9**, 3265; A. Zabala-Lekuona, J. M. Seco and E. Colacio, *Coord. Chem. Rev*., 2021, **441**, 213984.

2 M. S. Reis, *Coord. Chem. Rev*., 2020, **417**, 213357.

3 A. R. Rocha, V. M. García-Suárez, S. W. Bailey, C. J. Lambert, J. Ferrer and S. Sanvito, *Nat. Mater.,* 2005, **4**, 335; M. Affronte, *J. Mater. Chem*., 2009, **19**, 1731.

4 L. Bogani and W. Wernsdorfer, *Nat. Mat.,* 2008, **7**, 179; R. Vincent, S. Klyatskaya, M. Ruben, W. Wernsdorfer and F. Balestro, *Nature,* 2012, **488**, 357; M. Ganzhorn, S. Klyatskaya, M. Ruben and W. Wernsdorfer, *Nat. Nanotech*., 2013, **8**, 165; M. Jenkins, T. Hümmer, M. J. Martínez-Pérez, J. García-Ripoll, D. Zueco and F. Luis, *New. J. Physics*, 2013, **15**, 095007; V. Dediu, L. E. Hueso, I. Bergenti and C. Taliani, *Nat. Mater.,* 2009, **8**, 707; M. Prezioso, A. Riminucci, P. Graziosi, I. Bergenti, R. Rakshit, R. Cecchini, A. Vianelli, F. Borgatti, N. Haag, M. Willis, A. J. Drew, W. P. Gillin and V. A. Dediu, *Adv. Mater*., 2013, **25**, 534; M. Mannini, F. Pineider, C. Danieli, F. Totti, L. Sorace, P. Sainctavit, M. A. Arrio, E. Otero, L. Joly, J. C. Cezar, A. Cornia and R. Sessoli, *Nature*, 2010, **468**, 417; S. Thiele, F. Balestro, R. Ballou, S. Klyatskaya, M. Ruben and W. Wernsdorfer, *Science,* 2014, **344**, 1135; A. Cornia and P. Seneor, *Nat. Mater*., 2017, **16**, 505; S. Lumetti, A. Candini, C. Godfrin, F. Balestro, W. Wernsdorfer, S. Klyatskaya, M. Ruben and M. Affronte, *Dalton Trans.*, 2016, **45**, 16570.

5 M. N. Leuenberger and D. Loss, *Nature*, 2001, **410**, 789; M. J. Martínez-Pérez, S. Cardona-Serra, C. Schlegel, F. Moro, P. J. Alonso, H. Prima-García, J. M. Clemente-Juan, M. Evangelisti, A. Gaita-Ariño, J. Sesé, J. Van Slageren, E. Coronado and F. Luis, *Phys. Rev. Lett*., 2012, **108**, 247213; A. Gaita-Ariño, H. Prima-García, S. Cardona-Serra, L. Escalera-Moreno, L. E. Rosaleny and J. J. Baldoví, *Inorg. Chem. Front*., 2016, **3**, 568; G. Aromí and O. Roubeau, *Handbook on the Physics and Chemistry of Rare Earths*, Elsevier, 2019, **56**, pp. 1–54; D. Aguilà, O. Roubeau and G. Aromí, *Dalton Trans*., 2021, **50**, 12045.

6 D. N. Woodruff, R. E. P. Winpenny and R. A. Layfield, *Chem. Rev*., 2013, **113**, 5110; S. G. McAdams, A.-M. Ariciu, A. K. Kostopoulos, J. P. S. Walsh and F. Tuna, *Coord. Chem. Rev*., 2017, **346**, 216.

7 C. A. P. Goodwin, F. Ortu, D. Reta, N. F. Chilton and D. P. Mills, *Nature*, 2017, *548*, 439; F.-S. Guo, B. M. Day, Y.-C. Chen, M.-L. Tong, A. Mansikkamäki and R. A. Layfield, *Angew. Chem., Int. Ed*., 2017, **56**, 11445; F.-S. Guo, B. M. Day, Y.-C. Chen, M.-L. Tong, A. Mansikkamäki and R. A. Layfield, *Science*, 2018, **362**, 1400; C. A. Gould, K. R. McClain, D. Reta, J. G. C. Kragskow, D. A. Marchiori, E. Lachman, E.-S. Choi, J. G. Analytis, R. D. Britt, N. F. Chilton, B. G. Harvey and J. R. Long, *Science*, 2022, **375**, 198.

8 X.-L. Li, F.-Y. Min, C. Wang, S.-Y. Lin, Z. Liu and J. Tang, *Dalton Trans*., 2015, **44**, 3430; H. Tian, L. Ungur, L. Zhao, S. Ding, J. Tang and L. F. Chibotaru, *Chem. Eur. J*., 2018, **24**, 9928.

9 A. Bhunia, M. T. Gamer, L. Ungur, L. F. Chibotaru, A. K. Powell, Y.

Please do not adjust margins
Dalton Transactions

Journal Name

ARTICLE

Lan, P. W. Roesky, F. Menges, C. Riehn and G. Niedner-Schatteburg, *Inorg. Chem.*, 2012, **51**, 9589.

[10] S. K. Langley, D. P. Wielechowski, V. Vieru, N. F. Chilton, B. Moubaraki, B. F. Abrahams, L. F. Chibotaru and K. S. Murray, *Angew. Chem. Int. Ed.*, 2013, **52**, 12014.

[11] L. Ungur, M. Thewissen, J.-P. Costes, W. Wernsdorfer and L. F. Chibotaru, *Inorg. Chem.*, 2013, **52**, 6328.

[12] M. Coletta, S. Sanz, D. J. Cutler, S. J. Teat, K. J. Gagnon, M. K. Singh, E. K. Brechin and S. J. Dalgarno, *Dalton Trans.*, 2020, **49**, 14790; T. Rajeshkumar, R. Jose, P. R. Remya and Gopalan Rajaraman, *Inorg. Chem.*, 2019, **58**, 11927.

[13] M. Yonemura, Y. Matsumura, M. Ohba, H. Okawa and D. E. Fenton, *Chem. Lett.*, 1996, 601-602; E. Colacio, J. Ruiz-Sanchez, F. J. White and E. K. Brechin, *Inorg Chem.*, 2011, **50**, 7268.

[14] *CrysAlisPro Software System*, Agilent Technologies UK Ltd, Oxford, UK, 2012.

[15] *Bruker Apex2*, Bruker AXS Inc., Madison, Wisconsin, USA, 2004.

[16] G. M. Sheldrick, *SADABS, Program for Empirical Adsorption Correction*, Institute for Inorganic Chemistry, University of Gottingen, Germany, 1996.

[17] G. M. Sheldrick, *Acta Cryst.*, 2008, **64**, 112; G. M. Sheldrick, *Acta Cryst.*, 2015, **71**, 3.

[18] J. M. Soler, E. Artacho, J. D. Gale, A. Garcia, J. Junquera, P. Ordejon and D. J. Sanchez-Portal, *Phys.: Condens. Matter*, 2002, **14**, 2745.

[19] J. P. Perdew, K. Burke and M. Ernzerhof, *Phys. Rev. Lett.*, 1996, **77**, 3865.

[20] L. Kleinman and D. M. Bylander, *Phys. Rev. Lett.*, 1982, **48**, 1425.

[21] N. Troullier and N. J. L. Martins, *Phys. Rev. B*, 1991, **43**, 1993.

[22] R. Pollet and D. Marx, *J. Chem. Phys.*, 2007, **126**, 181102.

[23] M. Llunell, D. Casanova, J. Cirera, P. Alemany and S. Alvarez, SHAPE, v2.1, Barcelona, Spain, 2013.

[24] E. Colacio, J. Ruiz, G. Lorusso, E. K. Brechin and M. Evangelisti, *Chem. Commun.*, 2013, **49**, 3845.

[25] N. F. Chilton, R. P. Anderson, L. D. Turner, A. Soncini and K. S. Murray, *J. Comput. Chem.*, 2013, **34**, 1164.

[26] A. N. Georgopoulou, R. Adam, C. P. Raptopoulou, V. Psycharis, R. Ballesteros, B. Abarca and A. K. Boudalis, *Dalton Trans.*, 2010, **39**, 5020.

[27] V. Chandrasekhar, B. M. Pandian, R. Boomishankar, A. Steiner and R. Clérac, *Dalton Trans.*, 2008, 5143.

[28] J.-P. Costes, J. García-Tojal, J.-P. Tuchagues and L. Vendier, *Eur. J. Inorg. Chem.*, 2009, 3801.

[29] T. Yamaguchi, J. P. Costes, Y. Kishima, M. Kojima, Y. Sunatsuki, N. Brefuel, J. P. Tuchagues, L. Vendier and W. Wernsdorfer, *Inorg. Chem.*, 2010, **49**, 9125.

[30] I. Oyarzabal, B. Artetxe, A. Rodríguez-Diéguez, J. A. García, J. M. Seco and E. Colacio, *Dalton Trans.*, 2016, **45**, 9712.

[31] K. Kotrle, I. Nemec, J. Moncol, E. Čižmár and R. Herchel, *Dalton Trans.*, 2021, **50**, 13883.

[32] E. Cremades, S. Gomez-Coca, D. Aravena, S. Alvarez and E. Ruiz, *J. Am. Chem. Soc.*, 2012, **134**, 10532; E. Colacio, J. Ruiz, A. J. Mota, M. A. Palacios, E. Cremades, E. Ruiz, F. J. White and E. K. Brechin, *Inorg. Chem.*, 2012, **51**, 5857.

[33] F. S. Guo, Y. C. Chen, J. L. Liu, J. D. Leng, Z. S. Meng, P. Vrábel,

M. Orendáč and M. L. Tong, *Chem. Commun.*, 2012, **48**, 12219; H.-C. Hu, X.-M. Kang, C.-S. Cao, P. Cheng, B. Zhao, *Chem. Commun.* 2015, **51**, 10850; S. Zhang, W.-M. Wang, Y. Guo, C.-Y. Li, Y.-Y. Guo, Y.-L. Hou, *Polyhedron*, 2020, **191**, 114808; P.-F. Shi, C.-S. Cao, C.-M. Wang and B. Zhao, *Inorg. Chem.*, 2017, **56**, 9169; Y.-Y. Pan, Y. Yang, L.-S. Long, R.-B. Huang and L.-S. Zheng, *Inorg. Chem. Front.*, 2014, **1**, 649.

[34] J. Wu, X.-L. Li, L. Zhao, M. Guo and J. Tang, *Inorg. Chem.*, 2017, **56**, 4104.